Indian Journal of Pure & Applied Physics
Vol. 60, January 2022, pp. 16-22

Dependence of X-ray emission from Europa on solar activity cycle

Smart K B & C A Babu*

Department of Atmospheric Sciences, Cochin University of Science and Technology, Kochi - 682 016, Kerala, India

Received 24 November 2021; accepted 29 November 2021

The atmosphere of the Jovian Europa being tenuous, the interaction of the energetic solar photons is a probable source of excitation for the emission of X-rays from the surface of the satellite. Solar photons in the X-region of the electromagnetic spectrum have energies greater than the binding energy of the elemental constituents of the surface, cause excitation of electrons, and on de-excitation cause emission of X-rays through X-ray fluorescence. We developed models for the computation of the solar X-ray flux during the representative phases of a solar activity cycle (1-100 Å), and using these fluxes, we computed the photon-induced X-ray fluorescent and Rayleigh scattering emission flux from the regolith of the Europa by taking into account its predominant H_2O ice composition. This work observed that during the extreme case of the quiet Sun condition and an X2-class flare, the X-ray energy flux at the Europa distance of 4.96 AU vary from 1.08×10^{-7} to 5.23×10^{-4} ergs-cm^{-2}s^{-1}. This flux from the H_2O ice composition can generate a total X-ray energy flux, inclusive of the X-ray fluorescent and Rayleigh scattering events, varying as 1.40×10^{-23} to 6.21×10^{-20} ergs-cm^{-2}s^{-1}. These computed numbers of the X-ray energy fluxes at the telescope of the Chandra X-ray Observatory are of lesser magnitude in comparison to its observed numbers (3.0×10^{-16}). This deduction reveals the influence of a stronger excitation source than the photon-induced mechanisms of the generation of X-rays from the surface of the Europa.

Keywords: Solar corona; Europa; Tenuous; Exosphere; X-ray fluorescence; Rayleigh scattering

1 Introduction

The thin atmosphere of certain natural satellites in the Solar System lets direct interaction of the photons in the solar electromagnetic (EM) spectrum. The EM spectrum, the range of all possible energies/ wavelengths, arise due to the electronic transitions in atomic, molecular and nuclear systems. The spectrum in terms of energy is divided into radio wave (<10^{-5} eV), microwave (10^{-5}-0.01 eV), infrared (0.01-2 eV), visible region (2-3 eV), ultraviolet (3-10^3 eV), X-rays and γ-rays (> 10^5 eV). We focus in this work on the X-ray region of the EM spectrum, and X-rays originate from the electron shells of the atoms. Due to their penetrating abilities, the X-region (0.01-10 nm or 123.98 keV-0.12398 keV) is also classified as hard X-rays (0.01-0.1 nm; E > 12.4 keV) and soft X-rays (0.1-10 nm; E < 12.4 keV). The Sun and hot plasmas such as the stellar coronae are regarded as the traditional sources of X-rays in the Solar System. Burnight, 1949 reported the foremost detection of X-rays from the Sun on August 6, 1948, by the U.S. Naval Research Laboratory[2,3]. Ever after the discovery of the X-ray emission from the Comet Hyakutake[4], the Chandra X-ray Observatory (CXO) has discovered a remarkable array of planetary objects shining in soft X-rays. The planets [the Venus[5], the Earth[6], the Mars[7], the Jupiter[8], the Saturn[9]], the Moon[10,11], the comets[4] and even the asteroids[12] are also now known as soft X-ray emitters[13].

The Advanced CCD Imaging Spectrometer (ACIS) and High-Resolution Camera (HRC) are the focal plane science instruments of the CXO. The ACIS observed the Jupiter system during November 25-26, 1999, and the observations of the Imaging Array of the HRC-I was on December 18, 2000. The ACIS observation spanning 24 hours (86.4 ks) was in support of the Galileo flyby of the Io, and the HRC-I observation spanning 10 hours (36.0 ks) was in support of the Cassini flyby of the Jupiter[14]. The results of these seminal X-ray observations of the Jovian system reveal that the Io, the Europa and the Ganymede are also soft X-ray emitters (0.25-2 keV). Among them, this work focuses on the Europa and is inspired by its discovery as an X-ray emitter by the CXO[15]. In this context, we developed a model to compute the Kα X-ray energy flux generated from the surface of the Europa and detected at the telescope of the CXO due to the interaction of solar X-ray photons during different conditions of a solar activity cycle (ergs-cm^{-2}s^{-1}). The elemental composition of the

Corresponding author: (E-mail: babuca@cusat.ac.in)

surface of the tenuous Europa responds to the interaction of energetic solar X-ray photons through the emission of X-rays. Subsequently, this work developed computational models for the estimation of the photon-induced X-ray energy flux generated from the surface of the Europa for comparison with the observation of the CXO (ergs-cm^{-2}s^{-1}). The succinct description of the physical processes ensuing the photon interaction with the regolith of the Europa necessary for the computational aspects of the intensity of the X-ray photons generated from the surface and as observed by the telescope of the CXO is discussed (§2).

2 Materials and Methods

The Europa, the smallest among the Galileans, is currently geologically active, an ocean exists beneath its icy crust[16], the ocean remains liquid due to tidal flexing, and resurfacing is known to occur[17] which intersperse the subsurface oceanic material with the exogenic materials in the surface derived through the extra-planetary materials. The nominal surface age of the Europa is about 10-30 Ma[18,19], the measurements and mapping of the impact craters on the surface reveal that the ice shell is at least 19 kilometres thick[20], and Nimmo et al.[21] provide an estimate of a probable shell thickness of 25 kilometres. Models of the surface composition is the primal requirement for the quantitative analysis of the scenarios of X-ray emission from the surface of a satellite having a tenuous atmosphere. The thermal emission observations of the Galileo's photopolarimeter-radiometer show low-latitude diurnal brightness temperatures of the surface in the range of 86-132 K[22]. These temperatures favour the presence of H_2O ice. Even though the compounds and elements other than above are also probable in the surface composition of the Europa, we presently proceeded by considering H_2O ice as the predominant surface composition of the Europa, and envisage including an extended gamut of the probable elemental composition for implementation into the model simulations in a future paper.

2.1 Energetic photon fluxes in the environment of the Europa

The G2 star Sun is the primary source of energetics in the Solar System. The environmental species of solar origin that we took into account which can influence the surface energetics on the Europa is the energetic solar electromagnetic (EM) radiation. With a photospheric temperature of 6000 K, the Sun is hot enough to produce X-rays, and we took into consideration in this work only the X-region of the EM spectrum (1-100 Å). Its source region is the solar corona, and we considered the ever-pervasive solar coronal X-ray photons as the probable excitation source for the emission of X-rays from the surface of the Europa. The interaction of these energetic photons with the elemental composition of the surface of the Europa is envisaged in this work as responsible for the production of the observed X-ray emission from the satellite. Since the emission of the solar X-rays has a dependence on the solar activity cycle, this work also took into account the representative coronal conditions during a typical cycle of solar activity.

The solar coronal X-ray emission as the source flux consists of line and continuum emission, and the emission have a dependence on the solar activity cycle. Under the premises of an optically thin plasma whose electrons have Maxwellian energy distribution, we computed using the Chianti code the X-ray energy fluxes for the wavelength range 1-100 Å pertinent to the characteristic electron temperatures (T_e: 1-100 MK) and electron density (N_e) prevailing in the solar corona over a cycle of activity. For the computation of the solar coronal X-ray energy flux, we took into account a case of quiet Sun (SNo.1), two cases of A-class (SNo.2-3) and C-class flares each (SNo.4-5), three cases of M-class flares (SNo.6-8) and an extreme case of an X2-class flare (SNo.9). The representative numbers of the electron temperature (T_e) and the emission measure (cm^{-3}) adopted for the computation of the probable solar X-ray flux during these representative nine cases of a cycle of solar activity are discussed (Table 1).

We modelled the X-ray emission flux J(λ) from the quiet corona[23,24,25,26,27] using an electron temperature (T_e) of 1.50 MK and an emission measure of 1.0×10^{46} cm^{-3} (SNo.1). The progress in the solar cycle results in the emergence of sunspots (local regions of high magnetic field) first at high solar latitudes (~25^o N and S), advance nearer to the equator and later completely fade away at the end[28]. The bright areas (plages) which surround sunspot groups, coincide with the regions of enhanced field strength, these regions have lifetimes of days to months and are called active regions, where flares (transient outpourings of energy observable throughout the EM and particle spectrum) occur[29,30], and are characterized by a rise time on the order of

Table 1. — Cromer-Mann coefficients for elemental composition of Europa.

Cromer-Mann Coefficients	H (Z = 1)	O (Z = 8)
a1	0.490	3.049
b1	20.659	13.277
a2	0.262	2.287
b2	7.740	5.701
a3	0.197	1.546
b3	49.552	0.324
a4	0.050	0.867
b4	2.202	32.909
c	0.001	0.251

minutes and decay on the order of tens of minute. The flares are classified according to their strength. The least powerful and the faintest flares classified by the GOES 1-8 Å detector are the A-class (near background levels, 1-9 × 10^{-8} cm^{-3} Wm^{-2}) followed by B (background levels), C, M and X-class. The X-class is the biggest among the flares and is defined as an event during which the peak flux measured in the 1-8 Å waveband at the Earth is between 10^{-4}-10^{-3} W m^{-2}. The flux at the Earth of a flare of a given class is thus 10 times that of the previous class, and each class is divided into 9 sub-categories[28].

We modelled the X-ray emission flux (ergs-$cm^{-2}s^{-1}$) from the solar corona during the A-class flare for two instances[31,32]. The former is modelled using an electron temperature (T_e) of 8.00 MK, an emission measure of 1.0 × 10^{46} cm^{-3} (SNo.2), and the latter using an electron temperature (T_e) of 10.0 MK and an emission measure of 1.0 × 10^{46} cm^{-3} (SNo.3). The period of the observation of the CXO (November 25-26, 1999) belongs to the near maximum of the 23rd solar activity cycle[33,28]. The GOES observation of the X-ray flux during this period reveals that the dominant class of flares were of C-class. We modelled the X-ray emission from two C-class flares. The former has an electron temperature of 12.0 MK, an emission measure of 8.0 × 10^{46} cm^{-3} (SNo.4), and the second instant is modelled using an electron temperature of 12.30 MK and an emission measure of 9.0 × 10^{47} cm^{-3} (SNo.5). We modelled three M-class flares; the former has an electron temperature of 14.50 MK, an emission measure of 6.5 × 10^{47} cm^{-3} (SNo.6); the second has an electron temperature of 17.50 MK, an emission measure of 7.0 × 10^{48} cm^{-3} (SNo.7), and the third has an electron temperature of 24.0 MK and an emission measure of 7.0 × 10^{48} cm^{-3} (SNo.8). To model the emission flux during the X2-class of flare, we used an electron temperature of 25.0 MK and an emission measure of 1.0 × 10^{50} cm^{-3} (SNo.9).

2.2 Photon-induced X-ray emission fluxes from the Europa's surface

The X-ray fluorescence (XRF) spectrometry, since its primaeval inception onboard Apollo 15 mission on July 26, 1971, is traditionally used to investigate the elemental composition of the sun-lit landscapes of the tenuous planetary objects. Photo-absorption results in the ejection of electrons (photoelectric effect) and the subsequent emission of the photon is known as X-ray fluorescence (XRF). On the tenuous Europa, the interaction of the energetic solar coronal X-rays with their elemental composition is the causative factor for the emission of the fluorescent photons. The Rayleigh scattering is the process by which the bound atomic electrons scatter the photons, the process is elastic (photon energy remains unaltered), coherent (photon is scattered by the combined action of the whole atom), the atom is neither ionized nor excited, and cause background continuum for the fluorescent line emission[34]. For hard X-rays, the probability of the Rayleigh scattering is virtually negligible. We took into account in this work only the Rayleigh scattering process.

The intensity of the X-ray fluorescence from a surface $I_j(\lambda)$ is computed[35] with $J(\lambda)$ as the incident solar coronal X-ray flux, D as the distance from the Sun (AU), C_i as the mass fraction or concentration of each element, C_j that of the fluorescing element, and A_i denoting the relative atomic mass of the elements[36] in the surface composition by integrating from a minimum wavelength (λ_{min}) above which the fluorescence is empirically determined to become negligible to the K absorption edge (λ_K or E_K; E_K. λ_K = 12.4) as:

$$I_j(\lambda) = C_j \omega_j g_j J_K \frac{d\Omega}{4\pi D^2} \times \int_{\lambda_{min}}^{\lambda_K} \frac{J(\lambda)\cos(\alpha)\mu_{j_\lambda}}{\sum_i \left[C_i \mu_i(\lambda) + C_i \mu_i(\lambda_j)\frac{\cos(\alpha)}{\cos(\beta)}\right]} \mathrm{dE} \quad \ldots (1)$$

The intensity of the Rayleigh scatter at a particular wavelength $\sigma^R(\lambda)$ from the elemental composition of the surface of the Europa is modelled (eq. 2) under the premises of a homogeneous interior thicker than the interaction length of an X-ray photon[35,34,37]. With θ defined as the angle between the scattered radiation and the original incident radiation (scattering angle), we computed the efficiency factor (ξ_i) of the i^{th} element of Rayleigh scattering (eq. 3) with N_A as the Avogadro's number (6.022 × 10^{23} mol^{-1}), and A_i as

the relative atomic mass (mol^{-1}) in terms of the Rayleigh atomic DCS per unit solid angle for the elastic scattering of the unpolarized photons ($d_a\sigma_R/d\Omega$) through θ[34]. The exponential fit function[38,39] (eq. 4) with the notation θ denoting the Bragg angle (half the take-off angle of the spot), λ denoting the wavelength in Å, in the range of scattering vectors between $0 < (\sin\lambda < 2.0$ $Å^{-1}$, and the Cromer-Mann coefficients (a_i, b_i and c) is used to compute the atomic form factor F(x, Z) with x as the momentum transfer variable, Z as the atomic number of the nucleus of the target atom, and the computed numbers for the elemental composition of the Europa is presented (Table 1). The annular area ($d\sigma$) within which the deflection will be within a solid angle ($d\Omega$) and centred on the deflection angle is called the Differential Cross Section (DCS). With r_e (2.82×10^{-15} cm) as the classical electron radius[40], the electronic DCS for the Thomson scattering ($d_e\sigma_{Th}/d\Omega$) is averaged over the scattered-photon polarization in form factor approximation to compute:

$$\sigma_R(\lambda) = \xi_i \frac{d\Omega}{4\pi D^2} \times \int_{E_{min}}^{E_{max}} \frac{\Sigma_i^N J(\lambda)\cos(\alpha)\frac{C_i}{A_i}}{\Sigma_i^N\left[\mu_i(E_i)\,(1+\frac{\cos(\alpha)}{\cos(\beta)})\right]}\, dE \quad \ldots (2)$$

$$\xi_i = \frac{N_A}{A_i}\frac{da_R^\sigma}{d\Omega},$$

$$\frac{d\,a_R^\sigma}{d\Omega} = \frac{de_{th}^\sigma}{d\Omega}\,[F(x,Z)]^2 = \frac{r_e^2}{2}\,(1+\cos^2\theta)[F(x,Z)]^2 \quad \ldots (3)$$

$$f^o sin\frac{\theta}{\lambda} = \Sigma_{i=1}^4\,[a_i \exp\,(-b_i\left[\frac{\sin(\theta)}{\lambda}\right]^2)] \quad \ldots (4)$$

The various terms in these model expressions (eq. 1-4) can be understood in terms of the parameters that characterize the source excitation flux $J(\lambda)$, the medium and the detector. The source flux in the wavelength interval has units of ergs cm^{-2} s^{-1} $Å^{-1}$, and in the energy interval is ergs cm^{-2} s^{-1} keV^{-1}. The notation α denotes the primary X-ray incident angle to the normal (0^o at the sub-solar point). The strength of the source depends on the complement of the incident flux angle of the source. Hence, $J(\lambda)$ is multiplied by the cosine of α[35]; β is the complement of the exiting flux angle (0^o for the nadir-pointing instrument). Subsequently, for a sub-solar location with the detector pointing exactly at the nadir, we assumed in this work $\cos(\alpha)$ and $\cos(\beta)$ to be 0^o. The solid angle of the detector of the sensor is denoted as $d\Omega$. Among the photons generated from the surface, only a fraction is emitted towards the detector, and; if $d\Omega$ (sr) is the solid angle as viewed by the collimator-detector system, the fraction is obtained by dividing the solid angle by 4π to obtain the yield per unit solid angle[34].

The physical parameters required for the estimation of the intensity of XRF (eq. 1) is the absorption edges (K_{edge}), characteristic wavelengths ($K\alpha$), fluorescence yields (ω_K), transition probability ($g_{K\alpha}$), absorption jump ratio (r_K) or jump factor (J_K), absorption coefficients/ attenuation coefficients (μ). The fluorescence yield (ω) of an atomic shell or sub-shell is the probability that a vacancy in the shell under consideration will be filled by a radiative electron transition. The transition probability ($g_{K\alpha}$) is the fraction of the K_α photons in the total of X-rays emitted for the analyte. The K-shell absorption jump ratio (r_K) represents the probability that a K-shell electron will be ejected rather than an L- or M-shell electron. The probabilities r_K, ω_K and $g_{K\alpha}$ together is known as the excitation factor of the fluorescent X-rays [$Q_j(\lambda, \lambda_j)$]. The notation $\mu_i(\lambda)$ is the photo-attenuation coefficient, the absorption coefficient of the fluorescing element is denoted as $\mu_j(\lambda)$, and the notation $\mu_i(\lambda_j)$ denote the photo-attenuation coefficient of i^{th} element at the fluorescing wavelength of the fluorescing element. We obtained the current numbers of the parameters ω_j, g_j and r_j from the database *xraylib*[41]. The absorption and the attenuation coefficients (μ cm^2 g^{-1}) are computed using the desktop version of the NIST XCOM photon cross section database[42]. The absorption edges and the characteristic wavelengths are obtained from Bearden & Burr[43]. The K absorption edge energies (E_K) and the characteristic wavelength (K_α) of the elemental composition of the surface of the Europa are obtained from Bambynek et al.[44] and McMaster et al.[45] respectively.

3 Results and Discussion

The salient features of the solar coronal X-ray fluxes in the energy interval at the Europa distance of 4.96 AU (Fig. 1 and Table 2) during nine representative phases of a solar activity cycle and X-ray emission flux from the satellite as observed by the telescope of the Chandra X-ray Observatory (Fig. 2-5 and Table 3) are noted. The solar coronal X-ray energy flux during a case of the quiet sun (SNo.1) at the Europa distance of 4.96 AU is

Table 2 — Computed numbers of the Chianti solar X-ray flux at 4.96 AU (ergs cm^{-2} s^{-1}).

Solar Activity Phase	T_e (MK)	N_e (10^6 cm^{-3})	Energy Flux (ergs cm^{-2} s^{-1})
SNo. 1	1.50	2.659[a]	1.08E-07
SNo. 2	8.00	2.659[b]	1.44E-07
SNo. 3	10.00	2.659[b]	1.34E-07
SNo. 4	12.00	7.522[b]	8.70E-07
SNo. 5	12.30	25.229[b]	9.44E-06
SNo. 6	14.50	21.440[b]	5.20E-06
SNo. 7	17.50	70.360[b]	3.68E-05
SNo. 8	24.00	70.360[b]	3.68E-05
SNo. 9	25.00	265.935[b]	5.23E-04

Notes. - For the computation of the solar coronal X-ray energy flux (ergs cm^{-2} s^{-1}), we took into account a case of the quiet Sun [SNo.1, Leblanc & Le Squeren (1969); Acton (1996); Alexander (1999); Slemzin et al. (2014); Morgan & Taroyan (2017)], two cases of A-class (SNo.2-3) and C-class flares each (SNo.4-5), three cases of M-class flares (SNo.6-8), and an extreme case of an X2-class flare (SNo.9); b is from Feldman et al. (1996b, a). The representative numbers of the electron temperature (T_e) and the emission measure (cm^{-3}) adopted for the computation of the probable solar X-ray flux during these representative nine cases of a cycle of solar activity are discussed in §3.

Table 3 — Photon-induced integrated X-ray energy flux from the Europa (ergs cm^{-2} s^{-1}).

SNo.1	SNo.2	SNo.3	SNo.4	SNo.5	SNo.6	SNo.7	SNo.8	SNo.9
1.40E-23	6.00E-24	6.31E-24	4.68E-23	5.19E-22	3.40E-22	3.56E-21	4.20E-21	6.21E-20

Notes. - Integrated numbers in the energy interval are up to 12.4 keV. The descriptions for SNo.1-9 are the same as the notes in Table 2.

1.08×10^{-7} ergs cm^{-2} s^{-1}. The background levels of the X-ray energy flux modelled using two cases of the A-class flares at this distance is seen as varying from 1.34×10^{-7} to 1.44×10^{-7} ergs cm^{-2} s^{-1} (SNo.2-3). The X-ray emission flux generated by the two cases of C-class flares varies from 8.70×10^{-7} to 9.44×10^{-6} ergs-$cm^{-2}s^{-1}$ (SNo.4-5). We also note that a C-class flare having an electron temperature of 12.00 MK and an electron density of 2.520×10^7 cm^{-3} can generate an X-ray energy flux of 9.24×10^{-6} ergs-$cm^{-2}s^{-1}$. The X-ray energy flux generated by the M-class flares varies from 5.20×10^{-6} to 3.68×10^{-5} ergs-$cm^{-2}s^{-1}$ (SNo. 6-8). We also note that a case of X-ray active region emission from the whole Sun (T_e = 3.00 MK and $N_e = 5.980 \times 10^7$ cm^{-3}) can generate an X-ray energy flux of 3.85×10^{-5} ergs cm^{-2} s^{-1}, and a case of general corona (T_e = 1.50 MK and $N_e = 14.56 \times 10^7$ cm^{-3}) can generate 3.23×10^{-4} ergs cm^{-2} s^{-1}. The X-ray energy flux during the X2-class flare is 5.23×10^{-4} ergs cm^{-2} s^{-1} (SNo.9). Thus, it is observed that the solar coronal X-ray energy flux during these representative cases of a solar activity cycle at the Europa distance of 4.96 AU (Fig. 1) available for driving its surface energetics varies from 1.08×10^{-7} to 5.23×10^{-4} ergs cm^{-2} s^{-1} (Table 2).

The corresponding solar coronal energetic photon-induced X-ray energy flux generated from the Europa during the aforementioned nine representative phases of a solar activity cycle and as observed by the telescope of the Chandra X-ray Observatory

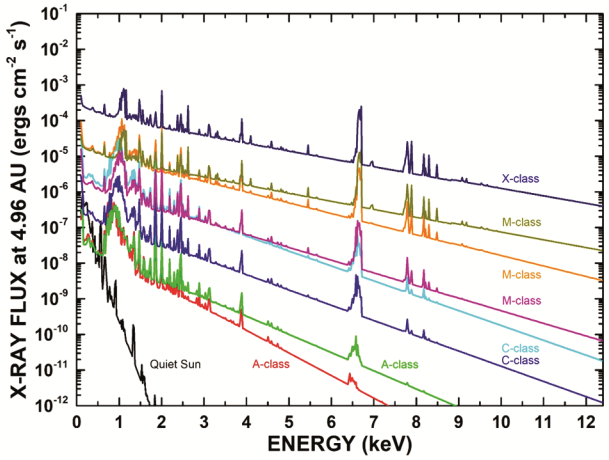

Fig. 1 — Solar coronal X-ray energy flux at the Europa distance of 4.96 AU.

(Fig. 2-5 and Table 3) are also noted. The comparative representation of the energy flux generated through the Rayleigh scattering during the quiet (Fig. 2) and the scenario of an extreme case of X2-flare (Fig. 3) reveal the enhancing of the contribution due to the elastic and coherent scattering during the flare situation and is seen as prominent beyond 0.5 keV. The comparative representation of the total X-ray energy flux (X-ray fluorescent + Rayleigh scattered) during the quiet (Fig. 4) and the scenario of an extreme case of X2-flare (Fig. 5) reveal the enhanced presence of scattering along with the predominant fluorescent emission from the oxygen atom. The energetic photon-induced X-ray emission

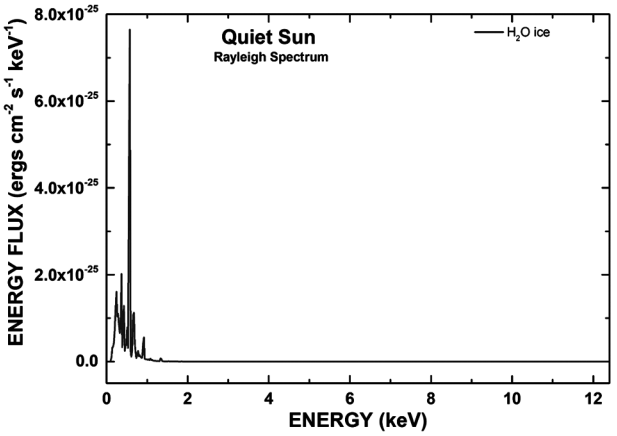

Fig. 2 — Rayleigh X-ray energy fluxes during quiet Sun at the CXO distance.

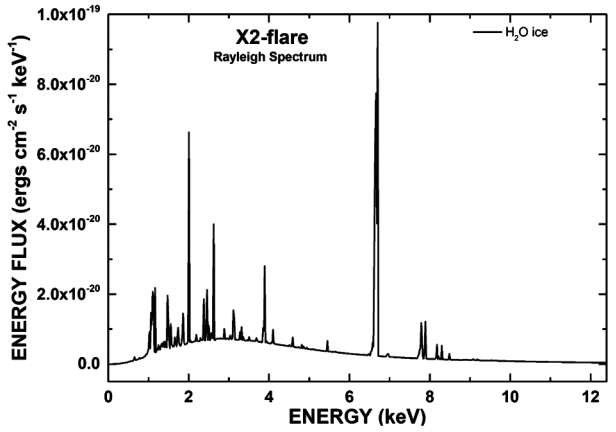

Fig. 3 — Rayleigh X-ray energy fluxes during an X2-flare at the CXO distance.

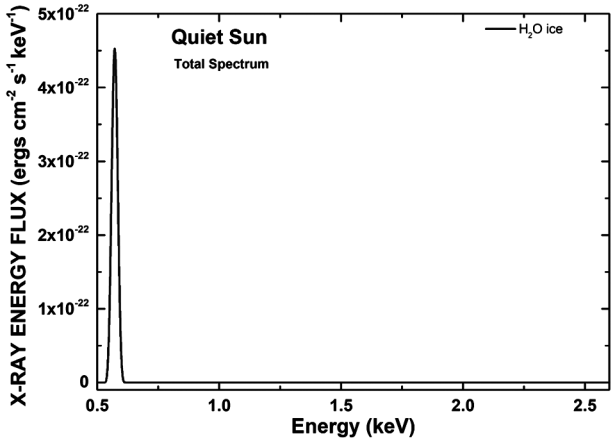

Fig. 4 — Total X-ray energy fluxes (XRF + Rayleigh) during quiet Sun at the CXO distance.

flux from the H_2O ice model of the surface of the Europa while the satellite is at 4.96 AU and received at the telescope of the Chandra X-ray Observatory during

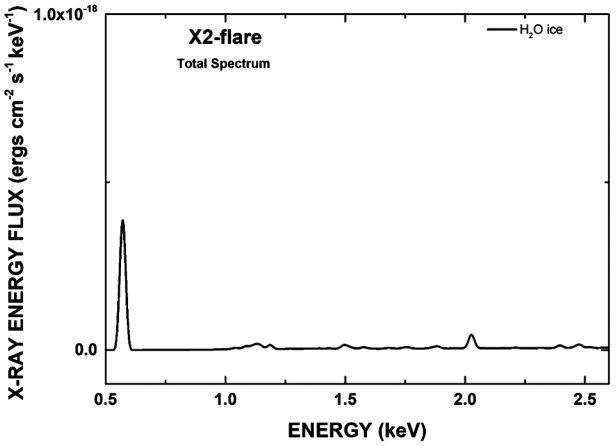

Fig. 5 — Total X-ray energy fluxes (XRF + Rayleigh) during an X2-flare at the CXO distance

the quiet coronal conditions (SNo.1) to an X2-class flare (SNo.9) of the solar cycle and as observed by the CXO varies from 1.40×10^{-23} to 6.21×10^{-20} ergs cm^{-2} s^{-1}. It is also observed that during the case of the quiet sun, the X-ray emission flux observed from the H_2O ice is 1.40×10^{-23} ergs cm^{-2} s^{-1}, and during the case of the X2-flare, the X-ray energy flux is 6.21×10^{-20} ergs cm^{-2} s^{-1}.

4 Conclusion

The comparative estimates of the numbers of the X-ray energy flux computed through numerical modelling undertaken in this work with the reported observations of the CXO reveal that the photon-induced emission process alone cannot generate the observed emission flux of X-rays from the Europa. Being completely engulfed within the magnetosphere of the Jupiter at 9.47 R_J ($R_J = 7.14 \times 10^4$ km), we propose the influence of the charged-particle interaction with the regolith of the Europa also as a probable mechanism for the emission of X-rays.

Acknowledgement

Smart K. B., one of the authors, is supported during the period of the doctoral studies by the U-JRF (Cochin University of Science and Technology); PURSE Programme of Department of Science and Technology, India, and; SRF through ISRO-PLANEX.

References

1 Burnight T R, *Phys Rev*, 76 (1949) 165.
2 Blake R L, Chubb T A, Friedman H & Unzicker A E, *Astrophys J*, 137 (1963) 3.
3 Culhane J L, *Mon Not R Astron Soc*, 144 (1969) 375.

4 Lisse C M, Dennerl K, Englhauser J, Harden M, Marshall F E, Mumma M J, Petre R, Pye J P, Ricketts M J, Schmitt J, Trumper J & West R G, *Science*, 274 (1996) 205.
5 Dennerl K, Burwitz V, Englhauser J, Lisse C & Wolk S, *Astron Astrophys*, 386 (2002) 319.
6 McKenzie D, Rugge H & Charles P, *J Atmos Terr Phys*, 44 (1982) 499.
7 Dennerl K, *Astron Nachr*, 324 (2003) 28.
8 Metzger A E, Gilman D A, Luthey J L, Hurley K C, Schnopper H W, Seward F D & Sullivan J D, *J Geophys Res Space Phys*, 88 (1983) 7731.
9 Branduardi-Raymont G, Bhardwaj A, Elsner R F & Rodriguez P, *Astron Astrophys*, 510 (2010) A73.
10 Adler I, Trombka J, Gerard J, Lowman P, Schmadebeck R, Blodget H, Eller E, Yin L, Lamothe R, Gorenstein P & Bjorkholm P, *Science*, 175 (1972) 436.
11 Adler I, Trombka J I, Schmadebeck R, Lowman P, Blodget H, Yin L, Eller E, Podwysocki M, Weidner J R, Bickel A L, Lum, R K L, Gerard, J, Gorenstein, P, Bjorkholm, P, & Harris, B, *Lunar and Planetary Science Conference Proceedings*, 4 (1973) 2783.
12 Lisse C M, Dennerl K, Englhauser J, Harden M, Marshall F E, Mumma M J, Petre R, Pye J P, Ricketts M J, Schmitt J, Trumper J & West R G, *Science*, 274 (1996) 205.
13 Nittler L R, Starr R D, Lim L, Mccoy T J, Burbine T H, Reedy R C, Trombka J I, Gorenstein P, Squyres S W, Boynton W V, Mcclanahan T P, Bhangoo J S, Clark P E, Murphy M E & Killen, R, *Meteorit Planet Sci*, 36 (2001) 1673.
14 Bhardwaj A, The Planetary X-ray Emission In: Gopalswamy N, Hasan S, Ambastha A (Eds) *Heliophysical Processes Astrophysics and Space Science Proceedings*, Springer, Berlin, Heidelberg, 2010, 271-282
15 Gladstone G R, Waite J H, Grodent D, Lewis W S, Crary F J, Elsner R F, Weisskopf M C, Majeed T, Jahn J M, Bhardwaj A, Clarke J T, Young D T, Dougherty M K, Espinosa S A & Cravens T E, *Nature*, 415 (2002) 1000.
16 Elsner R F, Gladstone G R, Waite J H, Crary F J, Howell R R, Johnson R E, Ford P G, Metzger A E, Hurley K C, Feigelson E D, Garmire G P, Bhardwaj A, Grodent D C, Majeed T, Tennant A F & Weisskopf M C, *Europa Io Plasma Torus Astrophys J*, 572 (2002) 1077.
17 Carr M H, Belton M J S, Chapman C R, Davies M E, Geissler P, Greenberg R, McEwen A S, Tufts B R, Greeley R, Sullivan R, Head J W, Pappalardo R T, Klaasen K P, Johnson T V, Kaufman J, Senske D, Moore J, Neukum G, Schubert G, Burns J A, Thomas P & Veverka J, *Nature*, 391 (1998) 363.
18 Squyres S W, Reynolds R T & Cassen P M, *Nature*, 301 (1983) 225.
19 Zahnle K, Dones L & Levison H F, *Icarus J*, 136 (1998) 202.
20 Phillips C B, McEwen A S, Hoppa G V, Fagents S A, Greeley R, Klemaszewski J E, Pappalardo R T, Klaasen K P & Breneman H H, *J Geophys Res: Planets*, 105 (2000) 22579.
21 Schenk P M, *Nature*, 417 (2002) 419.
22 Nimmo F Giese B & Pappalardo R T, *Geophys Res Lett*, (2003) 30.
23 Spencer J R, Tamppari L K, Martin T Z & Travis L D, *Science*, 284 (1999) 1514.
24 Leblanc Y & Lesqueren A M, *Astron Astrophys*, 1 (1969) 239.
25 Acton L, Comparison of YOHKOH X-ray and other solar activity parameters for November 1991 to November 1995 In Pallavicini R & Dupree A K (Eds), Cool Stars, Stellar Systems, and the Sun volume 109 of Astronomical Society of the Pacific Conference Series, (1996) 45.
26 Alexander D, *J Geophys Res Space Phys*, 104 (1999) 9701.
27 Slemzin V A, Goryaev F F & Kuzin S V, *Plasma Phys Rep*, 40 (2014) 855.
28 Morgan H & Taroyan Y, Sci Adv, 3 (2017).
29 Hathaway D H, *Living Rev Sol Phys*, 12 (2015).
30 Culhane J L & Acton L W, *Annu Rev Astron Astrophys*, 12 (1974) 359.
31 Toriumi S & Wang H, *Living Rev Sol Phys*, 16 (2019).
32 Hathaway D H, *Living Rev Sol Phys*, 12 (2015).
33 Feldman U, Doschek G A & Behring W E, *Astrophys J*, 461 (1996) 465.
34 Feldman U, Doschek G A, Behring W E & Phillips K J H, *Astrophys J*, 460 (1996) 1034.
35 Harvey K L & White O R, *J Geophys Res: Space Phys*, 104 (1999) 19759.
36 Hathaway D H, *Living Rev Sol Phys*, 12 (2015).
37 Ogawa K, Okada T, Shirai K & Kato M, *Earth Planets Space*, 60 (2008) 283.
38 Clark P E & Trombka J I, *J Geophys Res: Planets*, 102 (1997) 16361.
39 Wieser M E & Coplen T B, *Pure Appl Chem*, 83 (2010) 359.
40 Clark P E & Trombka J I, *J Geophys Res: Planets*, 102 (1997) 16361.
41 Ogawa K, Okada T, Shirai K & Kato M, *Earth Planets Space*, 60 (2008) 283.
42 Banerjee D & Vadawale S, *Adv Space Res*, 46 (2010) 651.
43 Ogawa K, Okada T, Shirai K & Kato M, *Earth Planets Space*, 60 (2008) 283.
44 Cromer D & Waber J, International Tables for X-ray Crystallography, The Kynoch Press: Birmingham, 4 (1974).
45 Hubbell J H, Veigele W J, Briggs E A, Brown R T, Cromer D T & Howerton R J, *J Phys Chem Ref Data*, 4 (1975) 471.
46 Mohr P J, Newell D B & Taylor B N, *J Phys Chem Ref Data*, 45 (2016) 043102.
47 Clark P E & Trombka J I, *J Geophys Res: Planets*, 102 (1997) 16361.
48 Ogawa K, Okada T, Shirai K & Kato M, *Earth Planets Space*, 60 (2008) 283.
49 Schoonjans T, Brunetti A, Golosio B, del Rio M S, Sol´e V A, Ferrero C & Vincze L, *Spectrochim Acta B*, 66 (2011) 776.
50 Berger M J & Hubbell J H, XCOM: Photon cross sections on a personal computer Technical Report NIST United States NBSIR, 87-3597 (1987).
51 Bearden J A & Burr A F, *Rev Mod Phys*, 39 (1967) 125.
52 Bambynek W, Crasemann B, Fink R W, Freund H U, Mark H, Swift C D, Price R E & Rao P V, *Rev Mod Phys*, 44 (1972) 716.
53 McMaster W H, Kerr Del Grande N, Mallett J H & Hubbell J H, *At Data Nucl Data Tables*, 8 (1970) 443.